Article

Enhancement of Distributed Temperature Sensitivity Using Al-coated Fiber in OFDR

Yong-seok Kwon,[1,2] Khurram Naeem,[1] Min Yong Jeon,[2*] and Il-Bum Kwon [1*]

[1] Center for safety measurement, Korea Research Institute of Standards and Science (KRISS), 267 Gajeong-ro, Yuseong-gu, Daejeon, Republic of Korea; kyss4133@kriss.re.kr; knaeem@kriss.re.kr

[2] Department of Physics, Chungnam National University, Daejeon 34134, Republic of Korea;

* *Correspondence: myjeon@cnu.ac.kr, ibkwon@kriss.re.kr .

Abstract: We present a distributed optical-fiber temperature sensor with enhanced sensitivity based on an Al-coated fiber using the Rayleigh backscattering spectra (RBS) shift in optical frequency-domain reflectometry (OFDR). The Al-coated sensing fiber with a higher thermal expansion coefficient compared to silica produces a strain-coupled shift in the RBS under an increase in temperature. This effect leads to an enhanced temperature sensitivity of the distributed measurement scheme. Our results revealed that the temperature sensitivity obtained using the Al-coated fiber in OFDR was ~56% higher relative to that of a single-mode fiber. Moreover, the minimum measurable temperature recorded was 1 °C with a spatial resolution of 5 cm.

Keywords: optical frequency domain reflectometry; distributed sensor; temperature sensor; tunable laser; coated fiber

1. Introduction

Distributed fiber optic sensors based on optical frequency domain reflectometry (OFDR) have been widely studied in the field of structural health monitoring (SHM) [1-4]. This is because OFDR techniques that exploit Rayleigh backscattering (RBS) in optical fibers offer several advantages over other distributed sensing schemes, such as, high spatial resolution, simple configuration, and faster measurement time (taking into account the time for data acquisition and processing). In particular, for optical sensing applications, a variety of OFDR sensors based on novel optical fibers with unique RBS features have been developed. These include high-birefringence fibers for simultaneous measurement of strain and temperature [5], air-hole microstructural fibers for high-temperature pressure sensing [6], Ge-doped core microstructural fibers for band-loss free measurement [7], fibers with thin film for magnetic field sensing [8], and polymer optical fiber for high strain sensitivity [9].

Distributed temperature sensing is important for various applications of SHM. The temperature sensitivity of OFDR based on a single-mode fiber (SMF) has been recorded to be ~1.3 GHz/°C [10]. Also, it was demonstrated that the temperature sensitivity of OFDR can be significantly improved by tapering the SMF or reducing the cladding diameter via etching [11, 12]. However, any structural modification of the fiber at multiple locations along the length not only induces loss of the OFDR signal, but also compromises the fiber's physical integrity and renders it unsuitable for deployment in practical applications of SHM. Usually, temperature sensitivity in optical fiber is based on the inherent effects of thermo-optic (TO) and thermal expansion (TE). To date, distributed fiber sensors based on

Preprints (www.preprints.org) | NOT PEER-REVIEWED | Posted: 31 May 2018 doi:10.20944/preprints201805.0477.v1

silica optical fibers primarily exploit TO effects for temperature measurement since the associated TE effect is too small and can be considered to be negligible. This fact limits the temperature sensitivity of OFDR sensors.

In this paper, we demonstrate a novel distributed temperature fiber optic sensor based on OFDR with enhanced sensitivity and resolution, using an Al-coated sensing fiber. When exposed to a temperature change, the Al-coating induces strain in the fiber due to its high TE coefficient in addition to the TO effect, thus leading to enhanced temperature sensitivity. The temperature sensitivity of the OFDR Al-coated was measured at 2.06 GHz /°C which is 40% and 56% higher than those of the fiber without the coating and SMF-28, respectively, while the spatial resolution was measured at 5 cm.

2. Experiments

Operation Principle and Experimental setup of the OFDR

Figure 1: Experimental setup of the OFDR using an Al-coated optical fiber. TLS is a tunable laser source which has ~100 kHz linewidth and a tuning wavelength range of 1440 nm to 1640 nm. C1, C2, C3 and C4 are optical couplers, PC is a polarization controller, PBS is a polarization beam splitter, PD is a photo detector.

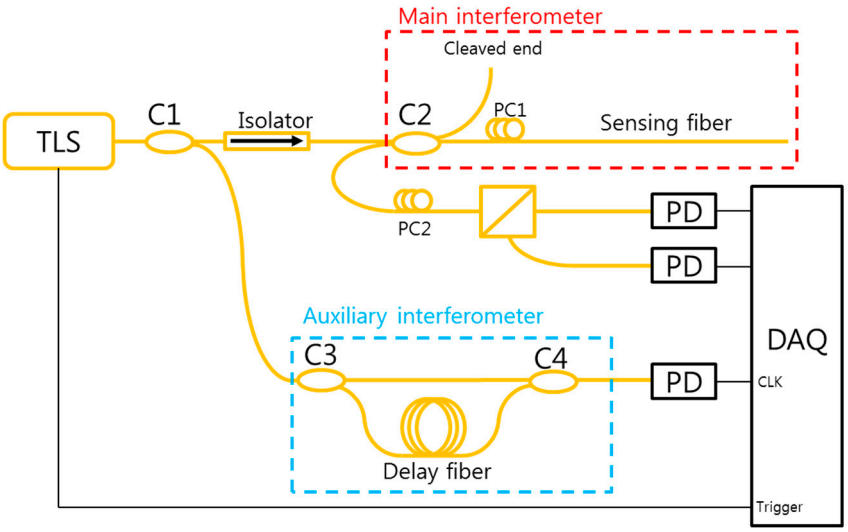

The proposed OFDR approach exploits RBS in an optical fiber. RBS is caused by the random modulation of the refractive index profile along the length of a fiber, and its amplitude is equivalent to that of a long and weak fiber Bragg grating with a random grating size. In OFDR, an external perturbation of the optical fiber at a given location causes a local change in the refractive index profile or the length of the fiber. In turn, this causes a shift in the optical frequency spectrum of the RBS in the local segment. For temperature measurement, the shift $\delta\nu$ in the optical frequency ν, of the RBS in response to the temperature change δT can be expressed as: [13]

$$-\frac{\delta\upsilon}{\upsilon} \approx (C_{TO} + C_{TE})\,\delta T \quad (1)$$

Where $C_{TO} = 8.6 \times 10^{-6}$ /°C and $C_{TE} = 0.55 \times 10^{-6}$ m/°C are the thermo-optic and thermal expansion coefficients for a standard optical fiber, respectively [13].

 doi:10.20944/preprints201805.0477.v1

Figure 1 shows the experimental setup of the OFDR which utilizes a polarization-diversity scheme [14]. An Al-coated optical fiber is used for sensing. Light launched from a tunable laser source (TLS, Agilent 8164B) is divided into two interferometers at a 1:99 fiber coupler, C1, where 99% of the light is sent to the main interferometer. The main interferometer is essentially a Michelson interferometer, which is made using a 3 dB 2×2 fiber coupler, C2. A sensing fiber is installed in one arm called the sensing arm, while Fresnel reflections occur at the cleaved end of the reference arm which constitutes a local oscillator (LO). After splitting equally at C2, the laser light scans the sensing fiber in a set optical frequency range. Spontaneous RBS light from the sensing fiber and Fresnel reflections from the LO arm are recombined at the same coupler C2, and this produces a beat signal in the frequency domain. This beat signal from the main interferometer is divided into orthogonally polarized components using an inline polarization-beam-splitter (PBS), and the output is detected using two photodetectors. Two polarization controllers (PCs) are used to optimize the signal to noise-ratio (SNR) of the RBS signal of the OFDR. PC1 is optimized to yield the maximum power of the RBS for the two orthogonal polarization states of *s* and *p* from the sensing fiber, while PC2 is optimized to equally divide the RBS light between the two polarization states of the PBS. An auxiliary interferometer is formed using two 3 dB fiber couplers C3 and C4 with a delay line of ~80 m in one arm. The auxiliary interferometer is important as it measures the instantaneous optical frequency of the TLS, with which we can remove the tuning nonlinearity of this device using a sampling clock signal that is generated at the same phase as the auxiliary Mach–Zehnder interferometer (MZI) beat signal generates the same frequency difference at each sampling point. One period of this beat signal has same frequency difference, so the same phase value implies the same frequency difference. The data acquisition (DAQ) board samples the beat signals of the main interferometer for *p*- and *s*-polarization using the sampling clock signal. This results in a corresponding beat signal with equal instantaneous frequency spacing. The application of Fast Fourier transform (FFT) to the sampled *p*- and *s*-polarization data facilitates the transformation into the length difference with LO and reflection of sensing fiber which called distance domain, and subsequently, the vector sum of the two FFT signals produces the OTDR-like loss-profile along the sensing fiber. The maximum length of the sensing fiber for distributed sensing is 20 m and is directly associated with the length of the delay fiber in the auxiliary MZI when sample once at one period of its interference signal. Thereafter, the sensing fiber is divided into many segments of equal length, and the application of the inverse FFT to the *p*- and *s*-polarization signals of each segment yields an associated local RBS spectrum in the frequency domain. Finally, to extract the local phase-shift induced by the temperature change, a cross-correlation analysis is performed between the RBS spectra (before and after sensing) of a segment, which demonstrates a shift in the optical frequency. Distributed temperature sensing can be achieved by calibrating this frequency shift.

Figure 2 describes the loss profile of the RBS signal along a sensing fiber consisting of a 6.11 m long Al-coated fiber. This fiber is made of an all-silica core (diameter ~ 9 μm) surrounded by a fluorine-doped silica cladding, and it is commercially available (artphotonoics, Germany). The loss in the Al-coated fiber is less than 1 dB/km. The fiber is perfectly fusion-spliced to the end of a lead-in SMF. Splicing between the two types of fibers was performed using a commercial fusion-splicer (FUJIKURA, FSM-30S) operating in automatic-mode without utilizing any special splicing conditions. The TLS was tuned at a speed of 1 nm/s over the wavelength of 1548 nm to 1553 nm during the state of the tuning process because the tuning non-linearity is large at the start of wavelength sweep. A 0.5 s trigger delay was also incorporated. It is clearly observed that the RBS signal exhibits a smooth intensity profile along the sensing fiber with a SNR of 15 dB.

Preprints (www.preprints.org) | NOT PEER-REVIEWED | Posted: 31 May 2018 doi:10.20944/preprints201805.0477.v1

Figure 2: Intensity profile of the RBS signal in an Al-coated optical fiber based on OFDR. Al-coated fiber starts at ~6.11 m location.

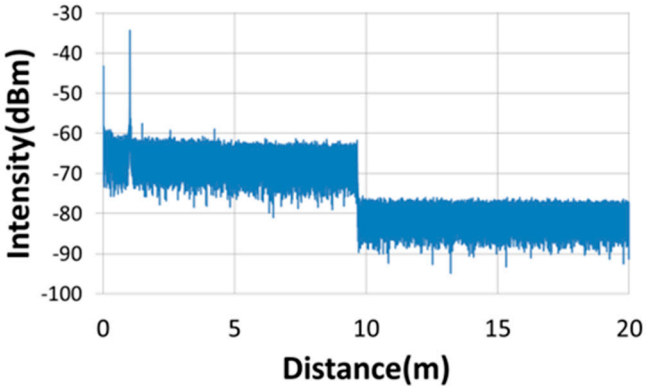

Figure 3: Relative shift of the optical-frequency under elevated temperature calculated from cross-correlation analysis with 5 cm spatial resolution along the (a) optical fiber with Al-coating, (b) optical fiber without Al-coating, and (c) SMF. (d) Linear measurement of the results in (a) –(c).

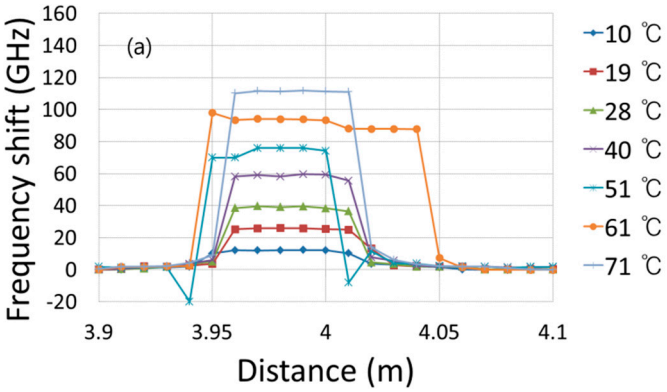

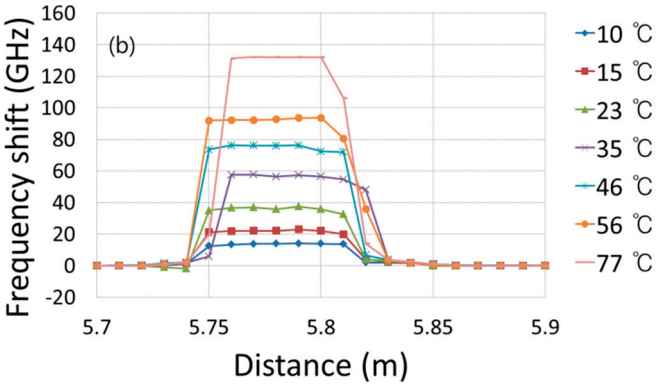

Preprints (www.preprints.org) | NOT PEER-REVIEWED | Posted: 31 May 2018 doi:10.20944/preprints201805.0477.v1

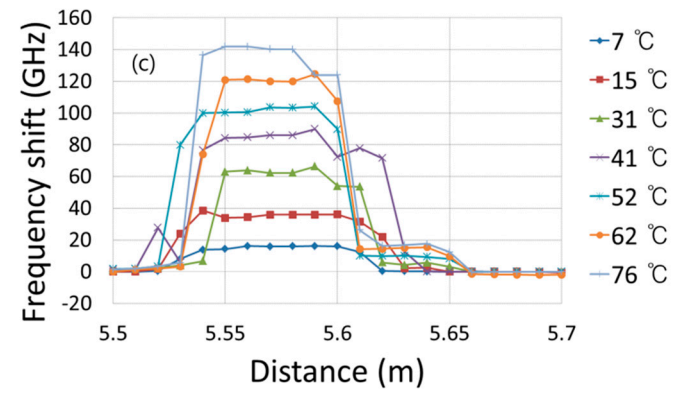

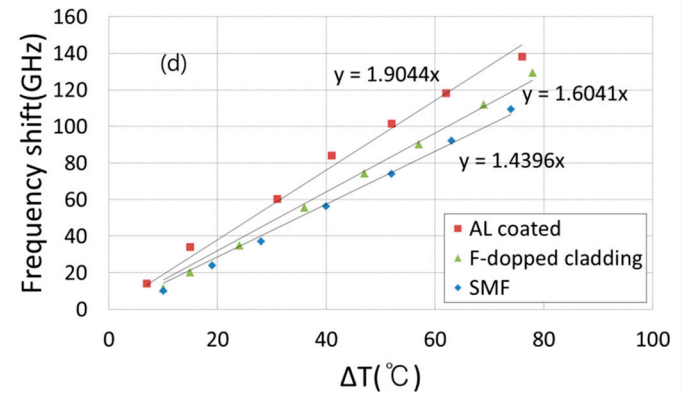

During the measurement process, distributed temperature sensing was performed using the Al-coated fiber with two types of temperature chambers. The first consisted of a small tube-type oven with a length of 5 cm and the second was a large commercial oven with a length of 1.7 m. Temperature sensing was also performed with the coating removed. In theory, the sweeping range Δυ, of the OFDR can be obtained using the spatial resolution of the OFDR measurement signal (Δz) as given by the relation, [1], where n_g is the group refractive index of the core-mode and c is the speed of light in vacuum. Since the measurement length of the sensing fiber (20 m) corresponds to half of the data size of the FFT signal in the distance domain, the experimental spatial resolution of the OFDR system can be easily determined from the ratio of the two as ~0.2 mm. Thus, the sweeping frequency range that is equivalent to a spatial resolution of Δz = 0.2 mm is about 500 GHz. Figure 3 describes the optical frequency shift of the cross-correlation analysis along the three types of fibers from 3.9 to 5.9 m length when a section of ~5 cm was exposed to an increasing temperature using the tube-type oven. We used a total of 250 data points (N) to generate a measurement segment for cross-correlation analysis. This implies that our OFDR system has a sensing spatial resolution of 5 cm (=N Δz) and the resolution of frequency shift is about 2 GHz (=Δν/N) per point. In Fig. 3(a), (b), and (c), the position of the optical frequency is presented for various temperatures of the Al-coated fiber, the fiber without the Al-coating and a standard SMF, respectively. The linear fitting of the average optical-frequency shift versus temperature for the temperature-change of 77 °C for the three types of fibers, is depicted in Fig. 3(d). The temperature spacing is difficult to control because the tube-type oven is controlled by a power supply and thermal heating coil. However, the frequency shift over the range of temperature change is linear and the temperature spacing difference does not matter. From Fig. 3, it can be seen that the temperature sensitivity of the fiber without Al-coating is 1.60 GHz /°C. This value increased by ~ 30% to 1.90 GHz/°C for the case of the Al-coated fiber. Note that the temperature sensitivity of the fiber

Preprints (www.preprints.org) | NOT PEER-REVIEWED | Posted: 31 May 2018 doi:10.20944/preprints201805.0477.v1

with/without Al-coating is about 40% / 10% better than that of a standard SMF which has a value of 1.439 GHz/°C. Taking into account the (2 GHz) resolution of the OFDR system, the temperature resolution values for the Al-coated fiber, without Al-coated fiber, and the SMF are computed to be 1.05 °C, 1.25 °C, and 1.39 °C, respectively. This confirms that temperature sensitivity and hence the resolution of the OFDR can be enhanced by using a fiber with Al-coating for which additional strain is induced upon heating due to the thermal expansion of the coating material.

Figure 4 describes the temperature measurement for the Al-coated fiber and the SMF with a 1.7 m long measurement length made of N= 8500 data points using a large temperature chamber. This implies that a resolution of the frequency shift of 0.06 GHz can be achieved. Thereafter, the 1.7 m long sections of the SMF and the Al-coated fiber were placed in the large temperature chamber as shown in the experimental setup in Fig. 4(a). Fig. 4 (b) presents the position of the optical frequency shift in the SMF (from 3.25 - 5 m) and in the Al-coated fiber (from 6. 85 - 8.6 m) when the temperature was gradually increased from 29 to 58 °C. It is clear that the optical frequency shift was larger in the case of the Al-coated fiber compared to the SMF. In this experiment, it can be stated that the temperature measurement range is from room temperature to 60 °C.

Figure 5 presents the result of resolving the optical frequency shift under a temperature change of 1 °C for the case of the SMF and the Al-coated fiber when the 1.7 m fiber section is heated in the large temperature chamber. In the cross-correlation analysis during signal processing, we used a sensing spatial resolution of 5 cm (N =250, resolution =1 °C), which is in line with our temperature measurement setup resolution of 1 °C. It can be observed that when the temperature was increased from 34 to 35 °C, the optical frequency shift for the cross-correlation analysis for the two temperatures was difficult to resolve in the case of the SMF. However, they were easily resolved in the case of the Al-coated fiber. This can be attributed to the temperature resolution of 1.05 °C for the Al-coated optical fiber, which is higher than that of 1.39 °C for the SMF case. We believe that by coating the sensing fiber with a material with a higher thermal expansion coefficient, the temperature sensitivity and hence temperature resolution can be improved further.

Figure 4: (a) Experimental setup for temperature measurement. (b) Relative shift of the optical-frequency under elevated temperature.

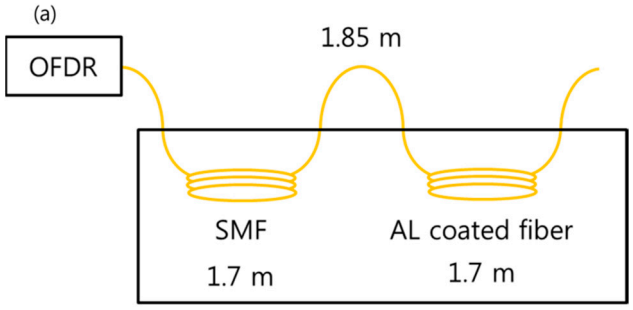

Preprints (www.preprints.org) | NOT PEER-REVIEWED | Posted: 31 May 2018 doi:10.20944/preprints201805.0477.v1

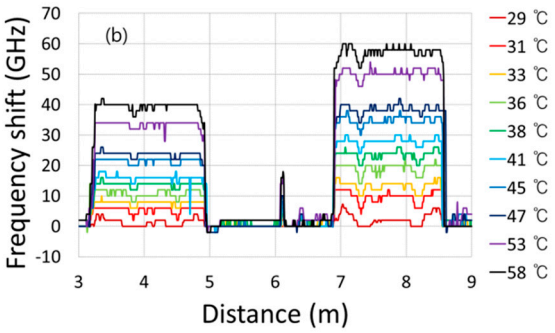

Figure 5: Resolving the shift of the optical frequency peak during cross-correlation analysis when the temperature is changed from 34 ° C (blue) to 35 ° C (red) in the case of (a) SMF, and (b) Al- coated fiber (see Fig. 4(b)).

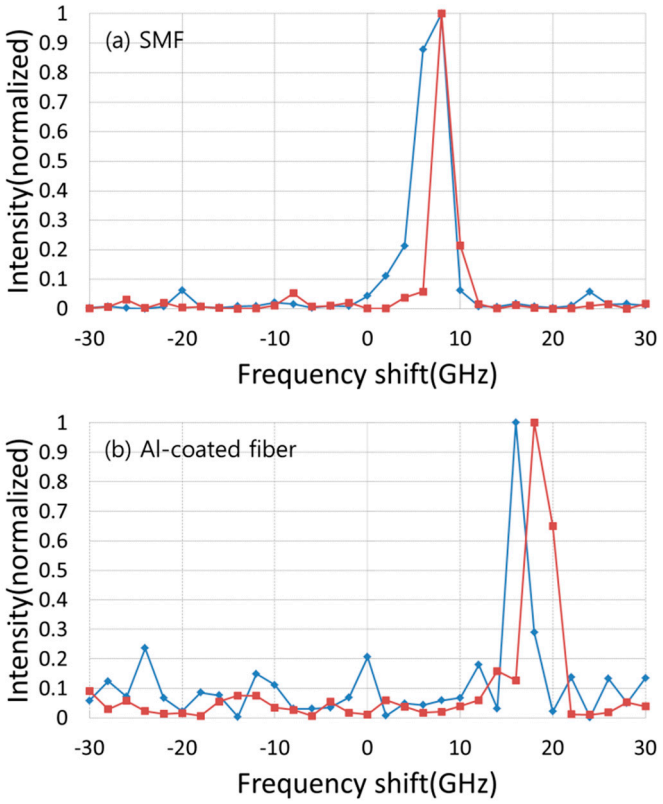

Figure 6: Relative shift of the optical-frequency under rising temperature.

Preprints (www.preprints.org) | NOT PEER-REVIEWED | Posted: 31 May 2018 doi:10.20944/preprints201805.0477.v1

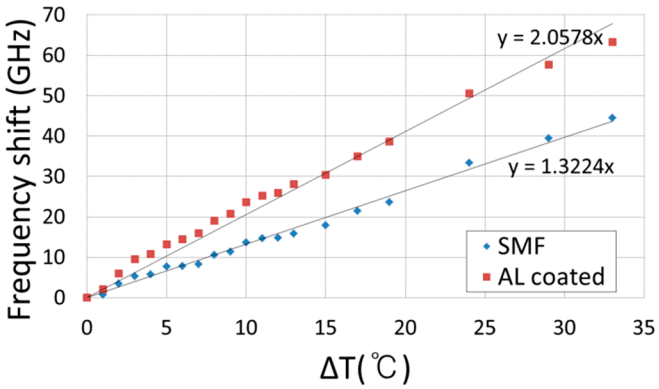

Figure 6 shows the average shift of the optical frequency with changing temperature for the Al-coated fiber and the SMF with a length of 1.7 m with a 5 cm segment size. The temperature sensitivity of the Al-coated fiber and SMF are estimated to be 2.058 GHz /°C and 1.32 GHz /°C, respectively, by linear fitting of the data in the temperature difference range up to 33 °C. It should be noted that, with the Al-coated fiber, the temperature sensitivity of the OFDR approach is improved by 56% compared to that of the SMF. The thermal expansion coefficient of Al is 24 × 10^{-6}/°C and that of fused silica is 0.55 × 10^{-6}/°C. In the axial direction, the expansion of Al is 24 μm/°C·m. This implies that 24 μ-strain is applied to the fiber per 1 °C. However this doesn't significantly increase the thermal sensitivity because radial expansion leads to negative pressure in the fiber which results in an opposite frequency shift compared to the strain and temperature change. During any measurements, the sensing fibers should be isolated from any environmental strain for accurate temperature measurement.

3. Conclusions

A distributed optical-fiber temperature sensor with enhanced sensitivity based on an Al-coated fiber using Rayleigh backscattering spectra shift in OFDR was demonstrated. The use of this fiber for temperature measurement resulted in an increase of the sensitivity by ~56% compared to the case of a SMF. The enhanced temperature sensitivity can be explained by the higher thermal expansion coefficient of the Al-coated fiber compared to that of the silica fiber, which causes a strain-coupled shift in the RBS under elevated temperatures. In the OFDR system, the temperature sensitivity is measured to be 2.06 GHz /°C which represents a 40% and 56% are improvement over the case of a fiber without coating and a SMF, respectively.

Acknowledgments

This research was supported by The Leading Human Resource Training Program of Regional Neo industry through the National Research Foundation of Korea (NRF) funded by the Ministry of Science, ICT and future Planning (NRF-2016H1D5A1909597), and also, supported by 'Intelligent safety diagnosis technology based on integrated measurement of micro/macro behaviors of public facilities' funded by Korea research Institute of Standards and Science. (KRISS-2016-16011040)

References

1. Bao, X.; Chen, L. Recent Progress in Distributed Fiber Optic Sensors. *Sensors,* **2012**, *12(7)*, 8601-8639
2. Zhou, D.; Li.; Chen, L.; Bao, X. Distributed Temperature and Strain Discrimination with Stimulated Brillouin Scattering and Rayleigh Backscatter in an Optical Fiber. *Sensors,* **2013**, *13(2)*, 1836-1845
3. Palmieri, L.; Schenato, L. Distributed Optical Fiber Sensing Based on Rayleigh Scattering. *The Open Optics J.,* **2013,** *vol. 7*, pp. 104-127
4. Wood, T. W.; Blake, B.; Blue, T. E.; Petrie, C. M.; Hawn, D. Evaluation of the Performance of Distributed Temperature Measurements With Single-Mode Fiber Using Rayleigh Backscatter up to 1000 °C. *IEEE Sensors J.*, **2014**, *vol. 14*, no. 1, pp. 124-128,
5. Li, W.; Chen, L.; X. Bao. Compensation of temperature and strain coefficients due to local birefringence using optical frequency domain reflectometry. *Opt. Commun.,* **2013,** *311(15)*, 26–32
6. Chen, T.; Wang, Q.; Chen, R.; Zhang, B.; Jewart, C.; Chen, K. P.; Maklad, Mokhtar.; Swinehart, P. R. Distributed high-temperature pressure sensing using air-hole microstructural fibers. *Opt. Lett.* **2012** *37*, 1064-1066
7. Naeem, K.; Kwon, Y. S.; Chung Y.; Kwon, I. B. Bend-loss-free distributed sensor based on Rayleigh backscattering in Ge-doped-core PCF. *IEEE Sensors Journal*, **2018,** *vol. 18*. 1903 - 1910 doi: 10.1109/JSEN.2017.2788017
8. Du, Y.; Liu, T.; Ding, Z.; Liu, K.; Feng, B.; Jiang, J. Distributed magnetic field sensor based on magnetostriction using Rayleigh backscattering spectra shift in optical frequency-domain reflectometry. *Appl. Phys. Express,* **2015,** *8* 012401
9. Liehr, S.; Wendt, M.; Krebber, K. Distributed strain measurement in perfluorinated polymer optical fibers using optical frequency domain reflectometry. *[J]. Meas Sci Technol*, **2010**, *21(9)*: 1–6. 2
10. Song, J.; Li, W.; Lu, P.; Xu, Y.; Chen, L.; Bao, X. Long-Range High Spatial Resolution Distributed Temperature and Strain Sensing Based on Optical Frequency-Domain Reflectometry. *IEEE Photonics Journal* **2014** *vol. 6*, no. 3, pp. 1-8.
11. Wang, X.; Li, W.; Chen, L.; Bao, X. Thermal and mechanical properties of tapered single mode fiber measured by OFDR and its application for high-sensitivity force measurement. *Optics Express*, **2012** *20 (14)*, 14779–4788,.
12. Ding, Z.; Yang, D.; Du, Y.; Zhou, Y.; Xu, Z.; Liu, K.; Jiang, J1.; Liu, T.; Note: Improving distributed strain sensing sensitivity in OFDR by reduced-cladding single mode fiber. *Rev. Scientific Instrum.*, **2016**, *vol. 87*, no. 12.
13. Chen, R.; Zaghloul, M.; Yan, A.; Li, S.; Lu, G.; Ames, B. C.; Zolfaghari, N.; Bunger, A. P.; Li, M-J.; and Chen, K. P. High resolution monitoring of strain fields in concrete during hydraulic fracturing processes. *Opt. Express*, **2016,** *vol. 24*, no. 4, pp. 3894-3902
14. Brian, J. S.; Dawn, K. G.; Matthew, S. W.; Mark, E. F. High resolution optical frequency domain reflectometry for characterization of components and assemblies. *Opt. Express,* **2005,** *13*, 666-674